AGU PUBLICATIONS

JGR

Journal of Geophysical Research: Atmospheres

RESEARCH ARTICLE
10.1002/2013JD020974

Key Points:
- Inception of subsequent strokes of natural bipolar cloud-to-ground flashes
- First report of inception mechanism of negative phase of bipolar CG flashes
- High-speed camera and multiple LLS study of bipolar CG flashes

Correspondence to:
A. C. V. Saraiva,
acvsaraiva@gmail.com

Citation:
Saraiva, A. C. V., et al. (2014), High-speed video and electromagnetic analysis of two natural bipolar cloud-to-ground lightning flashes, *J. Geophys. Res. Atmos.*, *119*, 6105–6127, doi:10.1002/2013JD020974.

Received 1 OCT 2013
Accepted 22 APR 2014
Accepted article online 28 APR 2014
Published online 28 MAY 2014

High-speed video and electromagnetic analysis of two natural bipolar cloud-to-ground lightning flashes

A. C. V. Saraiva[1], L. Z. S. Campos[1], E. R. Williams[2], G. S. Zepka[1], J. Alves[1], O. Pinto Jr.[1], S. Heckman[3], T. S. Buzato[1], J. C. Bailey[4], C. A. Morales[5], and R. J. Blakeslee[6]

[1]National Institute for Space Research, São José dos Campos, Brazil, [2]Department of Civil and Environmental Engineering, Massachusetts Institute of Technology, Cambridge, Massachusetts, USA, [3]Earth Networks, Germantown, Maryland, USA, [4]Earth System Science Center, University of Alabama in Huntsville, Huntsville, Alabama, USA, [5]Instituto de Astronomia, Geofísica e Ciências Atmosféricas, Universidade de São Paulo, São Paulo, Brazil, [6]NASA Marshall Space Flight Center, Huntsville, Alabama, USA

Abstract High-speed video records of two bipolar cloud-to-ground flashes were analyzed in detail. They both began with a single positive return stroke that was followed by more than one subsequent weak negative stroke. Due to the elevated cloud base height of its parent thunderstorm, the preparatory processes of each subsequent negative stroke were documented optically below cloud base. In the first event (Case 1) it was observed that all four subsequent negative strokes were initiated by recoil leaders that retraced one horizontal channel segment previously ionized by the positive leader. Those recoil leaders connected to the original vertical channel segment and propagated toward ground, producing four subsequent strokes that had the same ground contact point as the original positive discharge. The second event (Case 2), in contrast, presented 15 subsequent strokes that were initiated by recoil leaders that did not reach the original channel of the positive stroke. They diverged vertically toward ground, making contact approximately 11 km away from the original positive strike point. These results constitute the first optical evidence that both single- and multiple-channel bipolar flashes occur as a consequence of recoil leader activity in the branches of the initial positive return stroke. For both events their total channel length increased continuously at a rate of the order of 10^4 m s^{-1}, comparable to speeds reported for typical positive leaders.

1. Introduction

Bipolar lightning discharges are those that transfer both positive and negative electric charges to ground throughout their development. They are arguably one of the rarest types of lightning. In a review paper on this subject, *Rakov* [2003] discusses three basic categories of bipolar event. For upward and rocket-triggered lightning, he reports (i) events characterized by one or more polarity reversals during slowly varying current components [e.g., *McEachron*, 1939; *Hubert et al.*, 1984; *Waldteufel et al.*, 1980], (ii) events in which the initial-stage current and the following return strokes exhibit opposite polarities [e.g., *Berger and Vogelsanger*, 1966; *Nakahori et al.*, 1982], and finally, the focus of the present paper, (iii) those events that present return strokes of both polarities [e.g., *McEachron*, 1939; *Berger and Vogelsanger*, 1965; *Idone et al.*, 1987]. *Rakov* [2003] mentions that all documented discharges of the third type, at the time of publication, were of upward nature, with the exception of *Idone et al.* [1987]. They reported one case of triggered lightning initiated by the rocket-trailing wire technique that produced return strokes of both polarities. Lightning Location Systems around the world often observe flashes of opposite polarity that can be grouped as bipolar [*Schulz and Diendorfer*, 2003], according to the flash grouping algorithms commonly used [e.g., *Cummins et al.*, 1998]. Lastly, four recent published reports [*Fleenor et al.*, 2009; *Jerauld et al.*, 2009; *Nag and Rakov*, 2012; *Saba et al.*, 2012] document natural cloud-to-ground (CG) flashes that produce return strokes of both polarities.

Most studies in the literature (including the present work) report the majority of natural downward bipolar flashes starting with a positive discharge. The only exception is a recent paper by *Nag and Rakov* [2012], who reported two bipolar CG flashes starting with a negative stroke. *Fleenor et al.* [2009] presented conventional video records of four events that involved one initial positive stroke followed by one or two negative strokes. Of these four events two had the subsequent negative strokes retracing the preexisting channel created by the positive stroke. *Jerauld et al.* [2009] have observed one flash which consisted of two initial positive strokes followed by four negative strokes that occupied the same channel as the second positive stroke. Finally,

Saba et al. [2012] analyzed high-speed video and electric field records of two bipolar CG flashes initiated by a positive return stroke that was followed by one or two negative strokes.

The formation mechanism of natural downward bipolar flashes is briefly approached by *Saba et al*. [2012]. The authors suggest that the subsequent negative strokes are initiated by recoil leaders, according to the dart leader mechanism of the bidirectional leader concept [*Kasemir*, 1950, 1960; *Mazur*, 2002]. However, no conclusive optical evidence for this process has been reported.

The bidirectional leader model was first introduced by *Kasemir* [1950, 1960]. VHF mapping systems [*Shao et al*., 1995; *Rison et al*., 1999] provided observational support to the theory and suggested that dart leaders, responsible for initiating subsequent negative strokes, were initiated by K changes (or recoil leaders, as termed by *Mazur* [2002]). *Saba et al*. [2008] presented optical observations of recoil leaders during the development of downward positive leaders, showing that they develop through channel branches that were previously ionized by the positive leader, propagating in a retrograde fashion (i.e., toward the leader origin) with speeds of the order of 10^6 or 10^7 m s^{-1} and with durations no longer than 250 μs. *Mazur et al*. [2013, Figure 4] have presented optical evidence that recoil leaders develop bidirectionally, with its negatively charged end propagating toward the main positive leader while its positively charged end progressed in the opposite direction.

In a scenario where the positive return strokes initiate the bipolar CG flash sequence, thunderstorms capable of producing positive flashes in abundance are more suited to the occurrence of this kind of event. *Nag and Rakov* [2012] reviewed the storm scenarios favorable to the development of positive flashes and pointed out some cases: (1) tilted positive dipole, (2) positive monopole, (3) unusually large lower positive charge region, and (4) inverted dipole. *Williams and Yair* [2006] review the electrification processes that lead to the formation of the inverted polarity structures in thunderstorms. Its structure ideally has the polarity of the charge regions with opposite signs in comparison with typical thunderstorms [*Williams and Yair*, 2006; *Rust et al*., 2005]. Only a few studies attempt to identify this kind of thunderstorm [e.g., *Vonnegut and Moore*, 1958; *Williams and Boccippio*, 1993; *Kitagawa and Michimoto*, 1994; *Rust et al*., 2005; *Williams and Yair*, 2006].

In the present work we report high-speed camera records and electromagnetic data of two unusual bipolar CG events in which the initiation of the subsequent negative strokes is visible below cloud base. The optical signatures of the processes that initiate the subsequent strokes are similar to the recoil leader phenomenology present in the literature [*Mazur*, 2002; *Saba et al*., 2008; *Mazur and Ruhnke*, 2011; *Campos et al*., 2014].

2. Instrumentation and Data Description

During the summer of 2011/2012 the first lightning observation campaign of the RAMMER network (acronym in Portuguese for "Automatized multicamera network to observe and study lighting" [*Saraiva et al*., 2011]) was conducted in São José dos Campos, SP, Brazil. Over the same period, the CHUVA project (Cloud processes of the main precipitation systems in Brazil: A contribution to cloud resolving modeling and to the Global Precipitation Measurement [*Machado et al*., 2012]) installed several lightning detection systems covering the same region. The joint experiment led to a unique data set of lightning measurements. The cases presented here were observed by one RAMMER sensor and Brazilian Lightning Detection Network (BrasilDAT) network [*Naccarato et al*., 2012], with additional lightning location data from the CHUVA Vale do Paraíba experiment (Lightning Location Network (LINET), GLD360, and TLS200). Other networks that participated in the campaign also detected the same events, but these were the ones that provide peak current estimates as well. Information provided by the LMA (Lightning Mapping Array) network established for the CHUVA campaign was also used. The next sections will present a brief description of the instruments used in this analysis.

2.1. RAMMER Network

The RAMMER network was developed at the Brazilian National Institute for Space Research, sponsored by FAPESP (Fundação de Amparo à Pesquisa do Estado de São Paulo), beginning in late 2010. Each sensor consists of a high-speed camera, computer, GPS antenna, and some control circuitry. All equipment is stored in a weatherproof box, allowing it to be installed anywhere (Figure 1).

The camera is a Phantom V9.1, from Vision Research, and was configured for video records of 2 s duration at 2500 frames per second with a maximum exposure time of 390 μs. The spatial resolution is 1200 × 500 pixels, with 8-bit pixel depth (256 gray levels). This setup generates a video file of about 3 GB, and requires about 2 min to be transferred from the camera to the computer. During these 2 min no other flash can be recorded.

Figure 1. A RAMMER sensor (Phantom high-speed video camera on top with protective box for data computer below) located at site 2 (Vanguarda TV station tower).

Two sensors were installed in São José dos Campos during that summer season, and the operation began on 30 November 2011 and ended on 30 March 2012. Figure 2 shows the locations of the sensors during 13 March 2012, and the markers show the locations of case study strokes. As the events occurred behind the RAMMER 1 sensor, only RAMMER 2 was able to record them.

2.2. VLF/LF Lightning Detection Networks

For the return strokes recorded by the high-speed cameras, some had their locations and peak currents estimated by the Lightning Location Systems (LLS) in operation during that summer. Brazil has two low-frequency (LF)-based networks: Rede Integrada Nacional de Descargas Atmosféricas (RINDAT) (comprised of Vaisala sensors) and BrasilDAT (Earth Networks sensors). The LF-based networks provide estimates of location, time of occurrence, and return stroke peak current. Waveforms of the sensor closest to the events were retrieved from Earth Networks database, enabling us to recalculate peak currents more precisely and even estimate peak currents of strokes not detected by any other LLS that were operational during the CHUVA experiment. Moreover, during the CHUVA Geostationary Lightning Mapper (GLM) Vale do Paraiba campaign, LINET [*Betz et al*., 2004] and a TLS200 network (from Vaisala), were also installed. The Global Lightning Mapper (GLD)360 VLF network [*Demetriades et al*., 2010] also provides peak current estimates. Their data for the CHUVA period were also available for the project participants and used in this work.

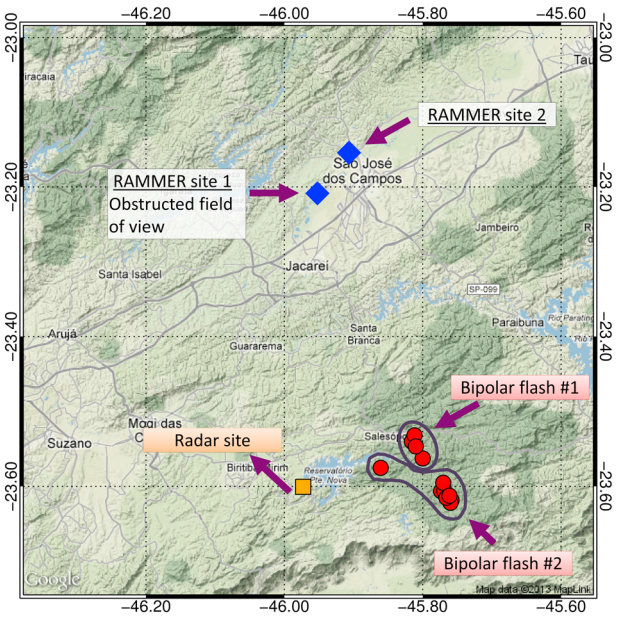

Figure 2. Relative locations of the camera observation site, radar, and the LLS solutions for the detected strokes of both analyzed events. The blue diamonds are the location of the RAMMER sites installed during the summer of 2011/2012. The red spheres are the estimated locations of each stroke of the bipolar CG flashes, and the yellow square is the location of the radar used in this work.

2.3. Lightning Mapping Array System

A temporary network of LMA receivers had been installed around the São Paulo metropolitan area during the 2011/2012 summer season. The network, named SPLMA, consisted of 12 sensors developed by the New Mexico Institute of Mining and Technology [*Rison et al*., 1999]. They were designed to detect lightning electromagnetic sources in the VHF range and locate them three dimensionally, making it possible to map the channel development both inside and outside the cloud. The SPLMA sensors used TV channels 8 (180–186 MHz) and 10 (192–198 MHz) to obtain the differences of time of arrival at each station with 80 μs resolution. Such data are used to locate the individual sources with roughly 50 m accuracy as long as they occur at distances less than approximately 150 km from the network center [*Rison et al*., 1999]. Both bipolar CG flashes analyzed in the present work occurred outside the network area, at distances ranging from 87 to 97 km from the LMA coordinate center. The closest

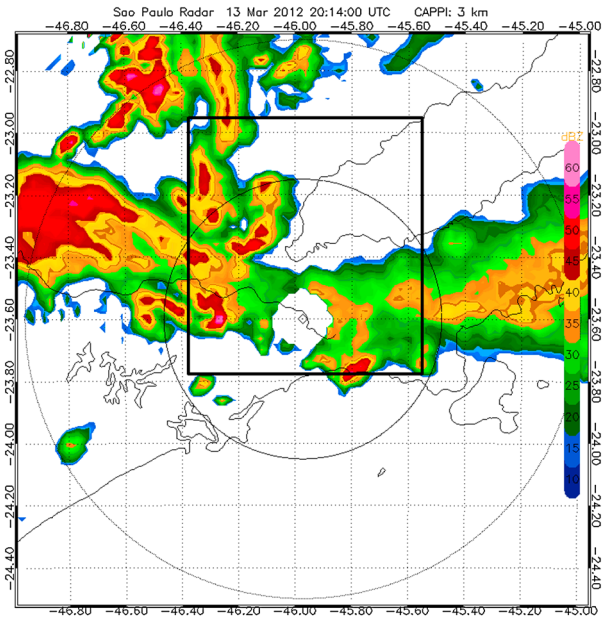

Figure 3. Constant Altitude Plan Position Indicator (CAPPI) at 3 km height less than 1 min after Case 2 was recorded, at 20:14:00 UTC. The black square indicates the same area presented in Figure 2.

sensors were between 34 and 45 km from the ground strike points of the individual strokes of each bipolar CG flash (based on the solutions included in the LLS data).

The SPLMA network was operated by NASA (National Aeronautics and Space Administration), University of Alabama in Huntsville, INPE (National Institute of Space Research), and USP (University of São Paulo) as part of the CHUVA experiment. The VHF source locations were used as complementary data to the high-speed video observations of the bipolar CG events detailed in the present paper.

3. Results and Analyses

During the day of 13 March, several single and multicellular thunderstorms formed in the observation region (over São Paulo metropolitan area and Vale do Paraíba). At 16:50 UT, a complex, multicellular thunderstorm began to develop northeast of the radar site and 50 km south of the camera site, in the form of an east-west oriented squall line. One hour later, the dimensions were ~100 km long and ~10 km wide. It continued to mature and by 18:39 UT had attained an area of about 4800 km^2. After that time, all cells near the radar site merged into a big cluster that only began to fade away after 00 UT on 14 March. From 17:00 to 23:00 UT, the RAMMER network registered a total of 44 CG flashes, the highest number for a single day during the campaign. However, the most impressive behavior occurred between 20:10 UT and 20:33 UT, when the camera registered two bipolar CG flashes in a 3 min interval, followed by four positive CG flashes. A sequence of so temporally close positive CG flashes, such as this, was never registered in that region during more than 10 years of high-speed camera observations. The camera observed no negative flash within this period, aside from the negative subsequent strokes in the bipolar CG flashes. All six flashes recorded in this period presented intense recoil leader activity visible below cloud base and, as discussed in the following sections, with some of them also responsible for the formation of subsequent negative strokes in the bipolar CG cases. Figure 3 is a radar CAPPI (Constant Altitude Plan Position Indicator) image at 20:14 UT, less than 1 min after the second bipolar CG flash that was recorded, showing the complex structure of the thunderstorm at that time, and the evidence for its east-west extension as a squall line.

A photogrammetry of the images, combined with the positions of the discharges estimated by the LLS, allowed the calculation of several parameters, like the cloud base height (above ground level) and channel length. The estimated cloud base height was 3.2 km, which is close to the value given by the nearby sounding (2.7 km), and also consistent with elevated cloud base heights in the case of mesoscale trailing stratiform regions [*Zipser*, 1977]. The channel length was calculated considering that the horizontal propagation of the channels is perpendicular to the line of sight for the camera detection. The viewing geometry led to perspective errors, and although the true angle from the detector is not known, the measured leader speeds (both positive and dart, see sections 3.1.1 and 3.2.1) are very similar to those reported in the literature [*Schonland et al*., 1935; *Orville and Idone*, 1982; *Jordan et al*., 1992; *Shao et al*., 1995; *Saba et al*., 2008; *Campos et al*., 2014], and therefore, the errors involved in this case should be small. Only the visible portion of the channel was considered in the calculations. BrasilDAT network data was used for location purposes for this analysis since its sensors are more uniformly distributed around the lightning events of interest than the other smaller networks that were operational during CHUVA. The average location error evaluated based on these events was around 1.5 km. The estimated ground strike point was 44 km from the camera, as calculated by using the LLS solutions and the GPS location of the observation site. Considering this distance, any uncertainties derived from LLS location errors should be less than 3%.

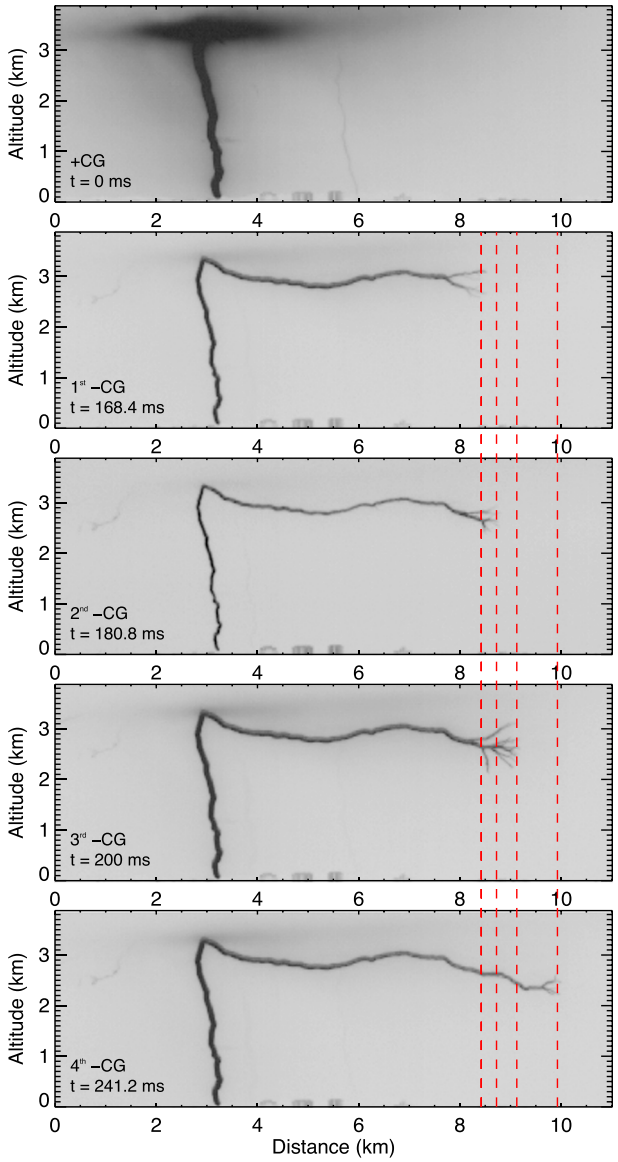

Figure 4. Selection of frame negatives for the return strokes comprising Case 1. The red dashed lines show the growth of channel length with time and stroke order.

The following sections will discuss in detail the formation and characteristics of the two bipolar CG flashes, which will be referred to as Case 1 and Case 2.

3.1. Case 1

3.1.1. Detailed Description

Case 1 occurred at 20:10:50 (UT) and was the first bipolar CG flash that could be recorded during the thunderstorm of interest, on 13 March 2012. An overview of selected video camera frames from Case 1 is presented in Figure 4, showing the visible channel of each return stroke. Figure 5 presents a timeline of Case 1, indicating the moment at which each return stroke occurred (with the initial positive stroke time $t = 0$ used as reference), as determined by the high-speed camera data, and the respective estimated peak current provided by BrasilDAT. In order to maximize the information provided by the BrasilDAT sensors, the waveforms corresponding to both cases were retrieved from the closest sensor to the lightning flashes for a thorough evaluation. Most of the strokes that were not reported by any LLS were identified on the waveforms and had their *E* field peak values used to estimate their corresponding peak currents. All recalculated peak currents for

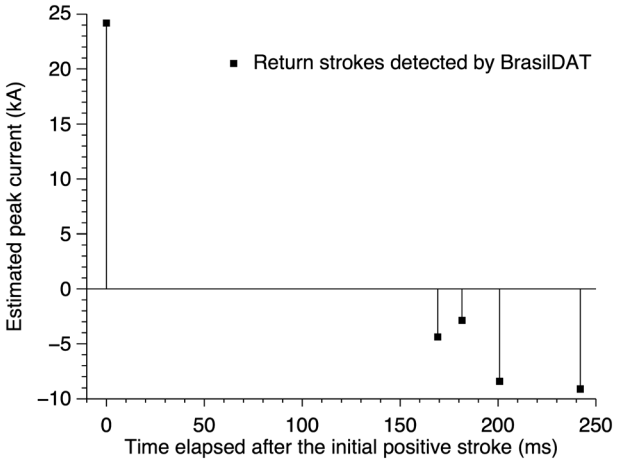

Figure 5. Timeline showing the instant of occurrence (determined from the high-speed video data) and the BrasilDAT estimated peak current for each return stroke that composes Case 1. Time $t = 0$ corresponds to the instant of occurrence of the initial positive stroke.

Case 1 are presented in Table 1. Figure 6 show the waveforms for all five strokes that compose Case 1. The waveforms also provide confirmation of the polarity change after the first positive return stroke.

The initial stroke of the flash was a positive return stroke, which was set up by a positive leader whose development was accompanied by a large number of recoil leaders visible below cloud base. Based on the camera observations, the return stroke occurred at approximately 20:10:50.944396 (UT). By matching the GPS timing between the camera and the LF networks down to 1 ms it was found that BrasilDAT provided a peak current estimate of +24 kA, GLD360 of +27 kA and TLS200 an estimate of +25 kA for the positive stroke. It was followed by a continuing current of approximately 33 ms (estimated by analyzing the remaining luminosity of the channel), which fits into the modal range of durations presented by *Saba et al.* [2010, Figure 6]. The estimated ground strike point was 44 km from the camera, as calculated by using the LLS solutions and the GPS location of the observation site.

While the continuing current of the positive stroke was still visibly active, some recoil activity started below cloud base and close to the channel to ground at time $t = 4$ ms (using the same reference as Figure 7). At time $t = 168.4$ ms the first negative return stroke was observed, initiated by one of the recoil leaders that could be observed approximately 2 ms prior to it. It was initiated in a horizontal channel branch that had been progressively developed by the propagating positive leader, as indicated by a large number of sequential recoil leaders that occurred at different moments after time $t = 4$ ms (when recoil activity became visible below cloud base). With the help of a luminosity versus time graph (presented in Figure 7, which was created using the same technique as *Campos et al.* [2009, 2013]), almost twenty individual recoil leaders could be identified to occur in channel segments that later on became part of the first negative stroke. Selected frames of two of these recoil leaders are presented in Figure 8. No clear tendency was noted for the recoil events to propagate progressively closer to ground; for instance, even after the example previously mentioned, it was possible to notice more than one recoil leader that reilluminated only the horizontal channel segment, among which some eventually moved toward cloud base. Finally, at $t = 166.0$ ms another recoil leader that propagated to the left reached the visible vertical channel segment that the initial positive stroke followed to ground. The leader then retraced it, touching the ground in the same strike point. This recoil event (that would normally be observed as a dart leader if its inception point was not visible below cloud base) had an approximate two-dimensional (2-D) speed of 4.5×10^6 m s^{-1} (typical for both recoil and dart leaders, as reported by *Saba et al.* [2008] and *Campos et al.* [2014], respectively). All six frames in which its development

Table 1. Summary of Characteristics of Each of the Four Return Strokes Observed in Case 1[a]

		I_p (kA)					
Order	Time of Occurrence (UT)	BrasilDAT	GLD360	TLS200	D (km)	L_{total} (m)	RL/DL Speed ($\times 10^6$ m s^{-1})
Positive	20:10:50.944 s ($t = 0$)	+24.2	+27.4	+25.0	43.9	3,480	N/A
1	51.113 s ($t = 168.4$ ms)	−4.38	N/A	N/A	46.7	8,890	4.45
2	51.125 s ($t = 180.8$ ms)	−2.87	N/A	N/A	N/A	9,100	7.58
3	51.144 s ($t = 200.0$ ms)	−8.43	N/A	−6.70	43.1	9,510	7.92
4	51.186 s ($t = 241.2$ ms)	−9.11	N/A	−7.60	44.8	10,450	1.31

[a] I_p corresponds to the peak currents, D is the distance between the strokes and the camera, L_{total} is the total visible channel length, and RL/DL speed is the estimated extension speed of the recoil/dart leader sequence that initiated each stroke. N/A stands for no data available.

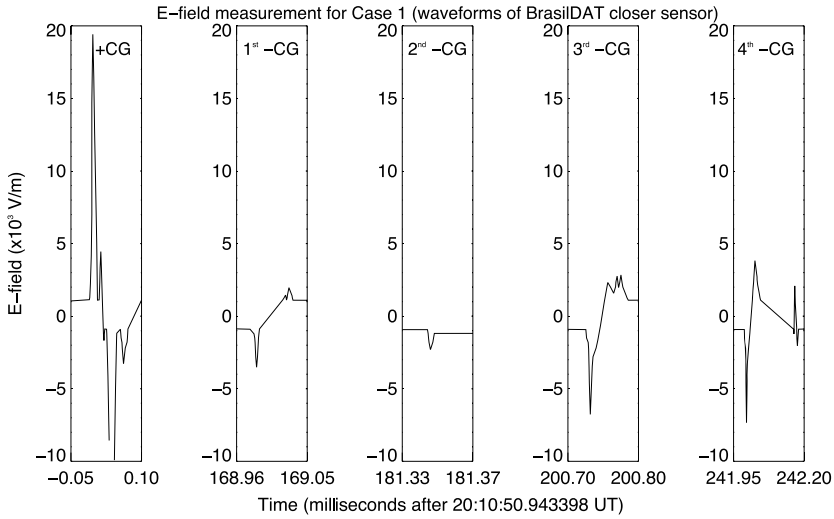

Figure 6. Electric field waveforms extracted from the BrasilDAT sensor that was closest to Case 1 ground strike point. Each graph shows a few microseconds of data for each return stroke.

can be seen are presented in Figure 9. A very short continuing current lasting approximately 2.4 ms followed the return stroke. BrasilDAT estimated that the return stroke peak current was close to −4.4 kA, but the other two LF networks did not detect it. Two-dimensional photogrammetry of the imagery provided an estimate of 8900 m for the total channel length (horizontal plus vertical segments), assuming that the entire visible channel was located on a plane parallel to the camera sensor.

Approximately 12 ms later, at time $t = 180.8$ ms (Figure 5), the second negative return stroke occurred, also following the same channel to ground as the initial positive stroke. It was also initiated by a visible horizontal recoil/dart leader in the same region of the previous one that began to propagate approximately 1.2 ms before the return stroke, presenting a 2-D speed around 7.6×10^6 m s^{-1} (also typical for both recoil and dart leaders). A continuing current lasting about 1.6 ms followed the return stroke. None of the three LF networks initially detected this return stroke, although, after the reanalysis of BrasilDAT sensor waveforms, its peak current was estimated as −3 kA, the smallest of all strokes. The total channel length was estimated to be roughly 9100 m, under the same assumption of the first negative stroke.

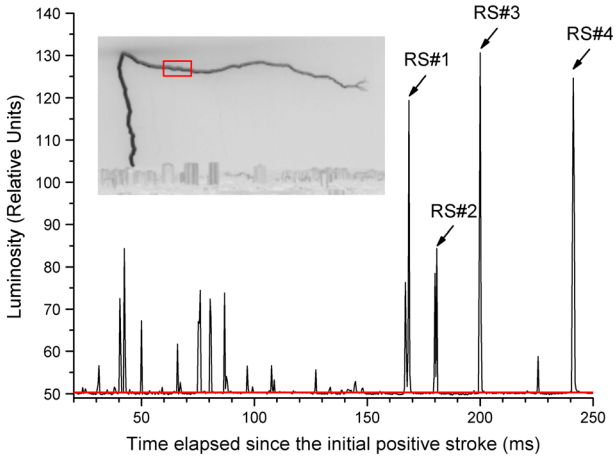

Figure 7. Luminosity versus time plot of the pixels located inside the red rectangle, showing the occurrence and relative intensity of the recoil leaders and negative subsequent strokes of Case 1 (indicated as RS#1 through RS#4).

The third negative stroke touched ground at $t = 200.0$ ms (Figure 5), initiated by a recoil/dart leader process 1.2 ms earlier that propagated with a speed of 7.9×10^6 m s^{-1}. Its inception occurred in the vicinity of the previous recoil/dart leaders but further away (about 6100 m) from the original vertical channel (of the initial positive stroke), presenting a visible channel with an estimated total length of 9500 m. Following the return stroke, a short continuing current lasting 2.4 ms could be observed by the camera. Neither LINET nor GLD360 detected the return stroke, but BrasilDAT and TLS200 did, providing peak current estimates of −8.4 and −6.7 kA, respectively.

Finally, the fourth and last negative return stroke occurred at $t = 241.2$ ms (Figure 5). It was also initiated by a recoil/dart leader

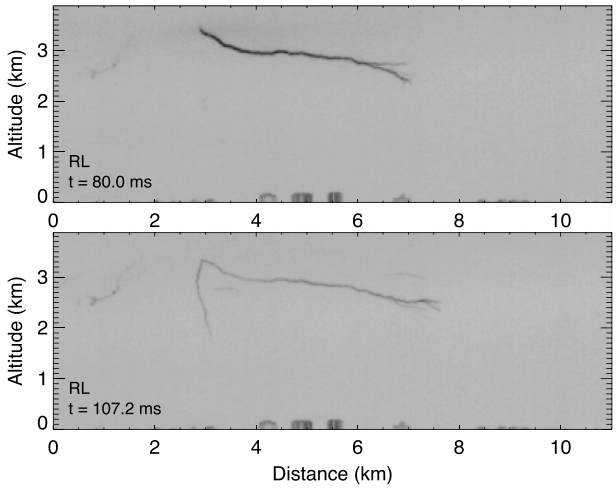

Figure 8. Example of two recoil leaders that precede the first subsequent negative stroke in Case 1, as observed by the high-speed camera. Both images are negatives of the originally recorded frames.

process, which lasted about 800 μs and propagated with an estimated 2-D speed of 1.3×10^7 m s^{-1}. This speed, similar to the process that initiated the third negative stroke, is also in good agreement with previous observations of both recoil and dart leaders. As observed in the previous strokes, the initial recoil development occurred still further away from the vertical segment of the channel, and the photogrammetric analysis provided an estimate of 10,500 m for its total length. The channel luminosity persisted for approximately 3.2 ms, again, indicating a very short continuing current. Only BrasilDAT and TLS200 detected the fourth return stroke, providing peak current estimates of −9.1 and −7.6 kA, respectively.

The general characteristics of each recoil/dart leader-return stroke sequence are summarized in Table 1. The evolution of the channel length with stroke order will be discussed in detail in the following section.

3.1.2. Analysis of Channel Length and Inferred Leader Speeds

Through a simple visual analysis of each return stroke frame (Figure 4) it was noticeable that the total channel length increased with stroke order as the recoil/dart leader processes had inception points progressively removed from the vertical segment created by the initial positive stroke. This evolution is presented graphically by Figure 10, which shows the total visible channel length versus time elapsed since the initial

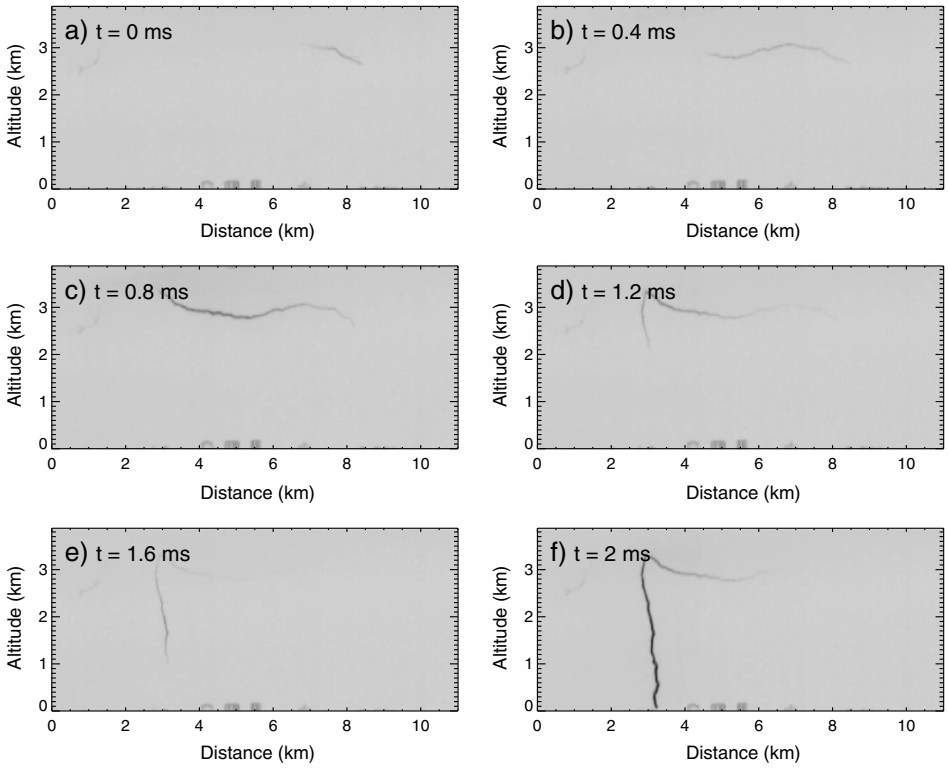

Figure 9. Complete high-speed video record of the recoil/dart leader that preceded the first subsequent negative stroke for Case 1. All the images are negatives of the originally recorded frames.

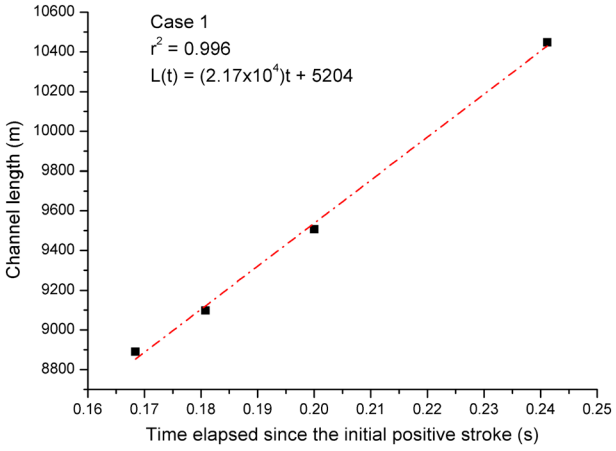

Figure 10. Total visible channel length (as estimated from the photogrammetric analysis) versus time elapsed since the initial positive return stroke for Case 1. Each square corresponds to one of the four negative strokes.

positive return stroke. Despite the small number of points available for Case 1 (only four), one can argue that there is a linear correlation between the two parameters. By fitting the data linearly, the obtained slope is 2.2×10^4 m s^{-1}, which can be interpreted as the speed with which that the recoil/dart leader inception points are moving away from the vertical channel segment, resulting in progressively longer channels as each subsequent stroke occurs. Given the statistical data presented by *Saba et al.* [2008] and *Campos et al.* [2014], this speed is in good agreement with the lower end of the distribution of natural positive leader speeds. It is also consistent with positive leader speeds measured from laboratory sparks [*Les Renardières Group*, 1977], triggered lightning experiments [*Kito et al.*, 1985], and individual natural events [*Kong et al.*, 2008]. Additionally, considering the evolution analysis of downward positive leader speeds with height made by *Campos et al.* [2014, Figure 12], one could argue that this value would be expected at greater heights, where the leader speeds seem to be smaller (approximately by 1 order of magnitude) than in the moments before making ground contact in a possibly stronger local electric field. The speed estimate is remarkably similar to the value obtained by *Waldteufel et al.* [1980] for the upward propagation of the stroke extremities of a triggered lightning flash that had its entire development visible below cloud base (3×10^4 m s^{-1}). *Krider* [1974] also estimated a similar propagation speed (1 to 4×10^4 m s^{-1}) for one long air discharge (about 16 km) visible below cloud base. Although the polarity of the leader could not be determined conclusively, the magnitude of its speed suggests positive polarity. Finally, even though a large correlation coefficient ($r^2 = 0.996$) was achieved in the linear fit that was applied to estimate the speed, it should be viewed with caution due to the limited sample size.

The photogrammetric analysis also allowed rough estimates of the average speeds of the recoil/dart leader processes of all the negative strokes of Case 1, listed in Table 1. They ranged from 4.5×10^6 to 1.3×10^7 m s^{-1}, in agreement with previous reports of both dart [*Schonland et al.*, 1935; *Orville and Idone*, 1982; *Jordan et al.*, 1992; *Campos et al.*, 2014] and recoil leader [*Shao et al.*, 1995; *Saba et al.*, 2008] speeds from digital high-speed cameras.

3.1.3. Discussion of the LMA Plots

The LMA sensors require direct line of sight from the lightning flash to achieve its maximum detection efficiency. The relatively large distance (approximately 92 km from the center of the network) and the terrain slopes between the core of the SPLMA network and the region where the bipolar CG events occurred likely caused a reduction in the number of VHF sources detected for these events. However, the resulting data still conveyed substantial information on the inception and in-cloud structure throughout the flash development.

Figure 11 shows plots of VHF sources mapped by SPLMA for Case 1. The cross symbols denote the location and/or time of occurrence of each return stroke, as provided by the both high-speed camera recordings and the solutions from the LF networks. The first noticeable feature is that the good position and timing match between the LF solutions and the distributions of VHF sources. The plot of source rate versus time shows that the majority of available points correspond to the in-cloud development of strongly VHF-emissive negative leaders as part of the bipolar formation of the initial positive return stroke. Even after the cessation of its continuing current (which lasted approximately 33 ms) and throughout the occurrence of the following four negative strokes, a large number of VHF sources are located above 5 km altitude (present in the number of sources versus height). The plots also show a considerable decrease in the number of sources approximately 10 ms prior to the first subsequent negative stroke at $t = 168.4$ ms. This suggests that there is no apparent connection between the negative strokes and the in-cloud development, or at least that their occurrence had no effect in intensifying it. The sources detected temporally close to the fourth subsequent stroke do not

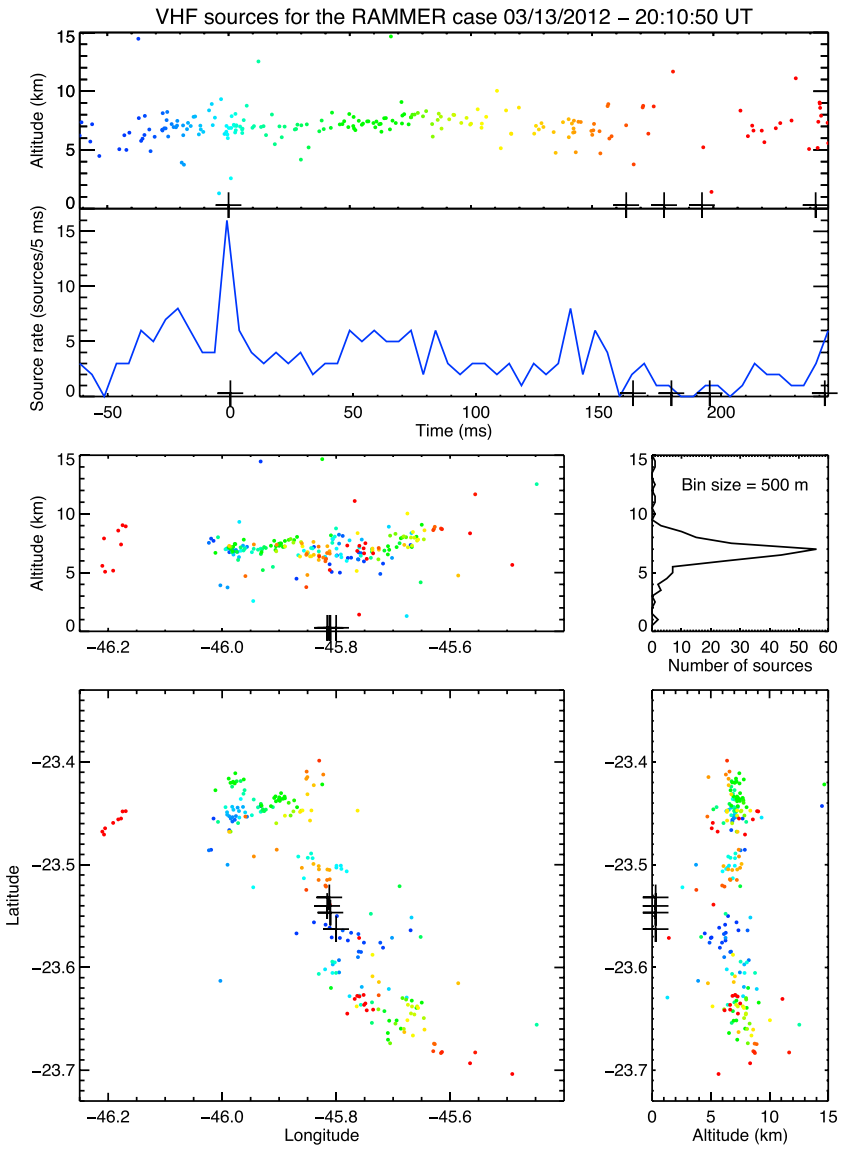

Figure 11. Plot of VHF sources produced by Case 1 and mapped by the SPLMA. Time progression is color coded according to the two topmost panels (altitude and source rate versus time plots). Each one of the other panels corresponds to spatial projections of the radiation source locations, and the cross symbols indicate the location and/or time of occurrence of each return stroke (provided by the high-speed camera and LF network solution data).

seem to be connected to it because of their spatial separation: there are no detections below 5 km and the latitude versus longitude diagram in Figure 11 indicates that they were produced further west from the ground contact points. This rough independence between strokes to ground and in-cloud development was also reached by *Krehbiel et al.* [1979, p. 21] and *Krehbiel* [1981, p. 224] for both intracloud and cloud-to-ground flashes based on multiple-station slow electric field data.

3.2. Case 2

3.2.1. Detailed Description

Case 2 began at 20:13:46 (UT) as the second bipolar CG flash observed by the RAMMER station camera. It occurred approximately 3 min later than Case 1, and given the time taken to record, save, and process the video file, the camera did not record any events in the period between the two events. However, the LLS data showed only one more CG flash (of positive polarity) between Case 1 and Case 2. Similar to Case 1, Case 2 was initially of positive polarity, with estimated ground contact (based on the camera records) at 20:13:45.905596 (UT) and was followed by 15 subsequent negative strokes. Figure 12 presents a selection of video frames showing

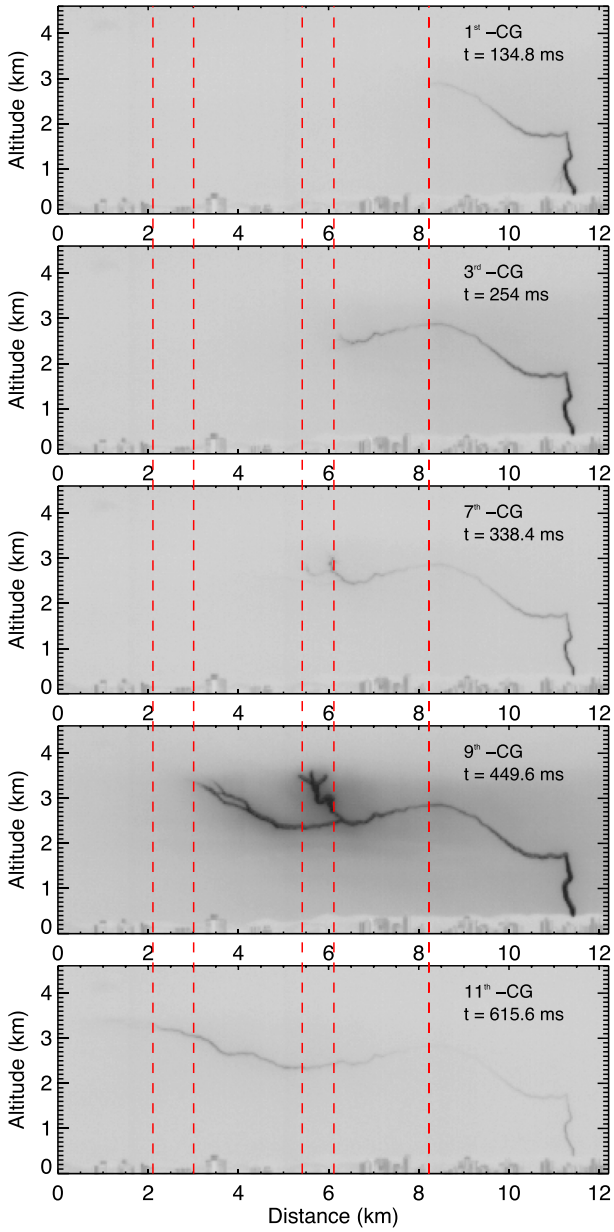

Figure 12. Selected negative frames of some of the negative strokes for Case 2. The red dashed lines show the growth of channel length with time and stroke order.

some of the return strokes that comprise Case 2. Similar to Case 1, the waveforms related to this flash were retrieved from a BrasilDAT sensor, and some of the waveforms are displayed in Figure 13, also confirming the change of polarity between return strokes. Figure 14 presents a timeline graph illustrating the instant each stroke occurred along with their respective estimated peak currents provided by BrasilDAT. Figure 15 presents a time-integrated image between the initial positive stroke (vertical channel, on the right-hand side) and the first negative stroke. Contrary to Case 1, the video record of the positive leader that produced the conductive path to ground did not show visible recoil activity below cloud base, possibly because of the larger distance from the camera. The four LF networks provided solutions for the positive stroke, whose ground contact point was estimated to be approximately 47 km away from the camera. The solutions included stroke peak current estimates: +25.6 kA by BrasilDAT, +44.1 kA by GLD360, +34.5 kA LINET, and +30.3 kA by TLS200. There was a persistence of the channel luminosity that lasted approximately 95 ms, very close to the median value for the duration of continuing currents of positive strokes (97 ms, according to *Saba et al.* [2010]). Visual analysis indicated at least three luminosity intensifications over the channel to ground that could be identified as positive *M* components [*Campos et al.*, 2009] and will be addressed in a future work.

Similarly to what was done in the discussion of Case 1, the instant the initial positive return stroke occurred will be taken as time $t = 0$. At $t = 134.8$ ms (roughly 40 ms after the cessation of the continuing current) another return stroke occurred, whose polarity will be discussed later in this section. During the time interval between the initial positive stroke (including the period of visibly active continuing current) and its first subsequent stroke, the camera indicated some recoil activity both within the cloud (mostly diffuse in the video camera imagery) and below its base (with discernible channels). A time-integrated image of the video frames recorded during that 134 ms long interstroke interval (presented in Figure 15) shows that part of the upper, horizontal section was traced by some of the recoil leaders that were produced as a consequence of the initial positive return stroke. Given the limited camera sensitivity, however, it is not possible to determine whether or not these recoil leaders created this new channel segment by themselves or if they were retracing branches originally produced by the first positive downward leader (as reported for some of the events studied by *Saba et al.* [2008, Figures 4b and 4c]) and that continued to develop further. The solutions provided by the LF networks indicate that the ground contact point of the first subsequent stroke was approximately 53 km from the camera and

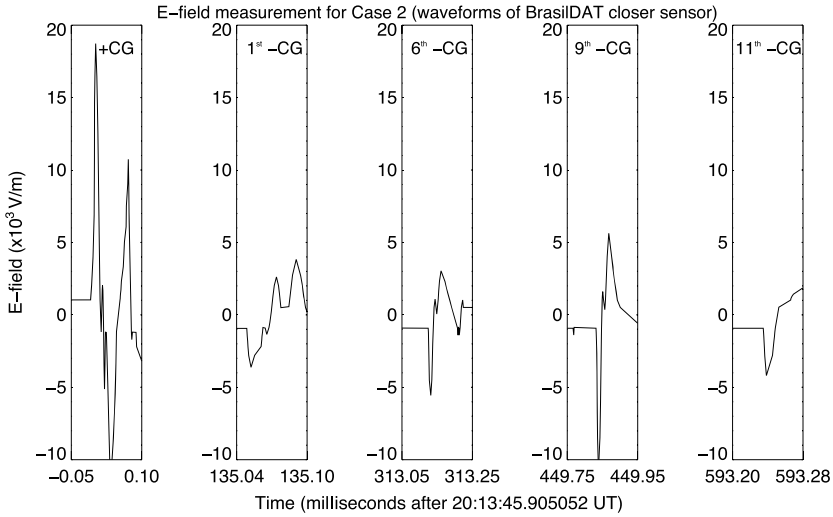

Figure 13. Same as in Figure 6 but only some of the return stroke waveforms for Case 2 are shown. The positive stroke is the first graph, followed by the first negative CG, then the 6th, 9th, and 11th −CGs. Note that the first −CG was misinterpreted by the LLS, but the waveform assures that it is a negative stroke.

separated from the initial positive stroke by about 11 km. The peak current information of BrasilDAT and LINET classified it as a positive ground discharge, while TLS200 identified it as a negative stroke (−5.2 kA). The waveform of Figure 13 shows that the *E* field of this stroke had a complex behavior, and probably, this was the reason the multiple LLS provided different results. However, the visual analysis of the waveform allowed the correct interpretation of the case and the conclusion that this was truly a negative return stroke, with peak current estimated in −5.5 kA. Photogrammetric analysis indicates that the total visible channel length is approximately 4700 m, assuming that its entire extension lies on a plane parallel to the camera sensor. Approximately 6 ms before the first subsequent return stroke, some recoil activity was visible, but the exact moment of the inception of the process that initiated the stroke could not be determined, and no estimates of its propagation speed were obtained.

The second subsequent stroke occurred at $t = 153.6$ ms in the same channel as the first. LINET, TLS200, and BrasilDAT reported estimated peak currents of −3.3, −3.0, and −3.2 kA, respectively. It was found that the total visible channel was roughly 5000 m long, but it was not possible to determine the recoil/dart leader propagation time and, subsequently, to obtain speed estimates.

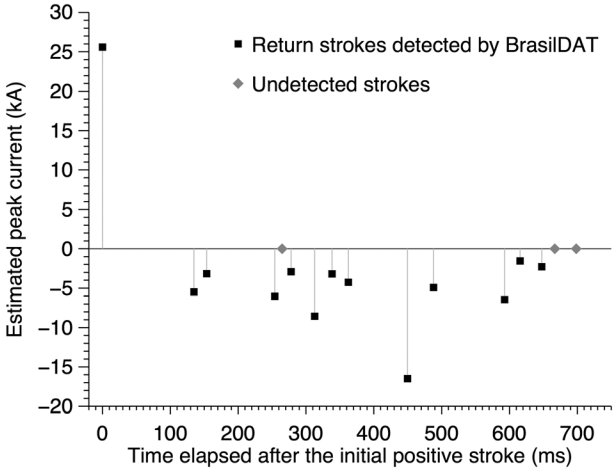

Figure 14. Timeline showing the instant of occurrence (determined from the high-speed video data), and the BrasilDAT estimated peak current for each return stroke that composes Case 2. Time $t = 0$ corresponds to the instant of occurrence of the initial positive stroke.

Contrarily to the previous return strokes, at $t = 248.8$ ms it was possible to observe the initiation of the recoil/dart leader process that produced the third subsequent stroke, which occurred at $t = 254.0$ ms. As the photogrammetric analysis provided an estimate of total channel length of 6700 m, this total development time would imply a propagation speed of 1.3×10^6 m s^{-1} (within the range of most common dart leader speeds, mentioned previously). All LLS provided solutions to the third stroke: GLD360 estimated a peak current of −5.7 kA, LINET a value of −6.1 kA, TLS200 a value of −5.3 kA, and BrasilDAT estimated the peak current in −6 kA.

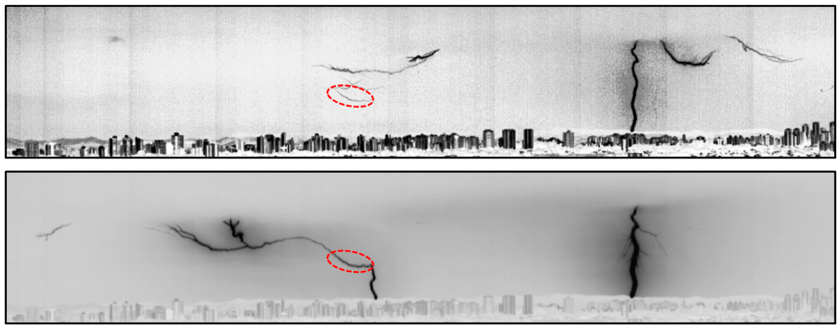

Figure 15. (top) Negative time-integrated image (with enhanced contrast) of the frames recorded during the 134 ms interstroke interval between the initial positive stroke (vertical channel on the right-hand side) and the first negative stroke (left-hand side). (bottom) Negative time-integrated image of all the video frames for Case 2. The channel segment that was illuminated by recoil leaders and was later part of the subsequent negative strokes is circled on both images.

Twelve return strokes followed the third, with parameters summarized in Table 2. For three among them, no peak current estimates were provided by any of the four LF networks. Through the video analysis, it is noticeable that their peak luminosities are considerably smaller than most of the other strokes (that could be confirmed by both camera and lightning location systems). It is possible that they are actually *M* components, even though the channel was too distant to allow the identification of preceding continuing currents following the previous strokes (apart from the initial positive stroke).

3.2.2. Analysis of Channel Length and Inferred Leader Speeds

Similarly to Case 1, visual inspection of the frames corresponding to each of the return strokes (Figure 12) suggested that the total channel length increased with stroke order. This evolution is presented graphically in Figure 16, which shows the total visible channel length versus elapsed time since the initial positive return stroke, using the same horizontal scale of the timeline graph (Figure 14 and Table 2). Given the relatively large number of available data points (one for each of the 15 subsequent negative strokes), the obtained linear correlation between the two parameters is even stronger than for Case 1. The slope obtained through fitting is 1.8×10^4 m s^{-1}, which, similarly to what was stated for Case 1, can be interpreted that the recoil/dart leader inception points are moving away from the vertical channel with that speed, which is also in good agreement with positive leaders observed in different circumstances.

Table 2. Summary of Characteristics of Each of the 16 Return Strokes Observed on Case 2[a]

Order	Time of Occurrence (UT)	Estimated Peak Current (kA)				D (km)	L_{total} (m)	RL/DL Speed ($\times 10^6$ m s^{-1})
		BrasilDAT	GLD360	LINET	TLS200			
Positive	20:13:45.906 s ($t = 0$)	+25.6	+44.1	+34.5	+30.3	47.1	3,290	N/A
1	46.040 s ($t = 134.8$ ms)	−5.47	N/A	+6.0	−5.2	52.5	4,670	N/A
2	46.059 s ($t = 153.6$ ms)	−3.18	N/A	−3.3	−3.0	N/A	5,020	N/A
3	46.160 s ($t = 254.0$ ms)	−6.03	−5.7	−6.1	−5.3	N/A	6,740	1.30
4	46.170 s ($t = 264.8$ ms)	N/A	N/A	N/A	N/A	N/A	7,080	4.43
5	46.184 s ($t = 278.0$ ms)	−2.93	N/A	−2.7	N/A	53.9	7,020	4.38
6	46.218 s ($t = 312.8$ ms)	−8.55	−11.0	−9.5	N/A	53.1	7,940	9.93
7	46.244 s ($t = 338.4$ ms)	−3.20	N/A	−3.5	N/A	54.2	8,120	6.77
8	46.268 s ($t = 362.4$ ms)	−4.27	−5.2	−5.0	N/A	52.3	7,920	4.95
9	46.355 s ($t = 449.6$ ms)	−16.5	−18.8	−18.5	−16.7	53.3	9,810	6.13
10	46.394 s ($t = 448.0$ ms)	−4.92	−8.6	−5.0	−4.4	51.0	10,870	9.06
11	46.498 s ($t = 592.8$ ms)	−6.44	−6.9	−6.7	−5.5	53.5	11,270	9.39
12	46.521 s ($t = 615.6$ ms)	−1.55	N/A	N/A	N/A	N/A	11,850	5.93
13	46.553 s ($t = 647.6$ ms)	−2.29	N/A	N/A	N/A	N/A	14,330	7.16
14	46.572 s ($t = 666.8$ ms)	N/A	N/A	N/A	N/A	N/A	14,980	6.24
15	46.604 s ($t = 698.4$ ms)	N/A	N/A	N/A	N/A	N/A	15,000	N/A

[a] I_p corresponds to the peak currents, D is the distance between the strokes and the camera, L_{total} is the total visible channel length, and RL/DL speed is the estimated extension speed of the recoil/dart leader sequence that initiated each stroke. N/A stands for no data available.

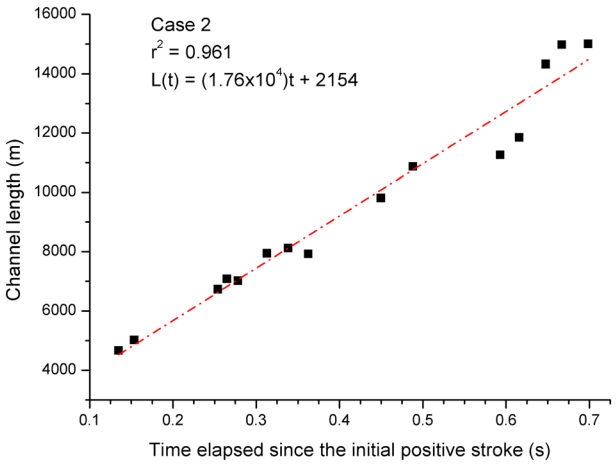

Figure 16. Total visible channel length (as estimated from the photogrammetric analysis) versus time elapsed since the initial positive return stroke for Case 2. Each square corresponds to one of the 15 negative strokes.

An analysis of Figure 16 and Table 2 shows that between some subsequent strokes, the inferred change of channel length does not seem to follow the overall trend. This is the case when strokes 3–5 are considered independently, and also strokes 6–8 (strokes 5 and 8, particularly, presented shorter channels if compared to their immediately previous strokes). Despite these anomalous points, the linear fit applied to all the data points has a notably high correlation coefficient ($r^2 = 0.96$), showing that the growing trend was present during the entire flash development.

From the third to the fourteenth stroke, it was possible to estimate the propagation time spent by the recoil/dart leader to touch ground. By combining that information with the photogrammetric analysis, it was possible to obtain average 2-D speeds for those events. The values are listed in Table 2, and they ranged from 1.3×10^6 to 9.9×10^6 m s^{-1}, also in agreement with the available information on both dart and recoil leaders.

3.2.3. Discussion of the LMA Plots

The positive stroke and the subsequent negative strokes of Case 2 occurred approximately 87 and 97 km away from the center of the LMA sensor network, respectively. The relatively large distance and the terrain slopes between the core of the SPLMA network and the region where the bipolar CG events occurred possibly caused a reduction on the expected number of VHF sources to be detected for these events (more information about the SPLMA installed during the CHUVA campaign can be found in *Bailey et al.* [2011]). Also, similar to Case 1, the resulting data have provided relevant information on the inception and in-cloud development of each individual stroke.

Each individual VHF source that could be detected by SPLMA during the time span of Case 2 is plotted on Figure 17. On each of three sections the cross symbols indicate the location and/or time of occurrence of each individual stroke, estimated from the combined information of the high-speed video data and the solutions provided by the LF networks. In the altitude versus longitude and the latitude versus longitude diagrams, it is noticeable that the majority of sources detected before the first subsequent negative stroke were mapped in the vicinity of the initial positive stroke, spreading mostly to the west and above 4 km. This in-cloud structure is likely to be related to the negative end of the double-ended tree that ionized the conductive channel to ground in the initial positive stroke. The altitude versus time diagram and source rate (number of sources per 10 ms) versus time plot indicate that the number of VHF sources falls dramatically with the negative stroke order. It is reduced to practically none after the sixth touches the ground, suggesting that their channel development below cloud base is completely disconnected from any persisting negative leader branches associated with the inception of the initial positive stroke. This is more evident than the similar behavior reported for Case 1 in section 3.1.3 probably due to the large difference in their multiplicities. No individual sources could be related to the recoil/dart leader processes that initiated each of the 15 subsequent negative strokes, possibly due to the fact that their inception occurred below 2.5 km (as indicated by the photogrammetric analysis). The very few sources detected around that height were displaced either spatially or temporally from the ground contact point and/or time of occurrence of the negative strokes.

The conclusion of the LMA analysis, for both cases, indicates that the positive strokes played a fundamental role in the formation of the negative strokes on the bipolar CG flashes. However, after their initiation, the negative strokes behave like an independent negative CG flash, but in a smaller scale, and are no longer connected to the development of the in-cloud negative leader of the double-ended tree associated with the bidirectional inception of the initial positive stroke.

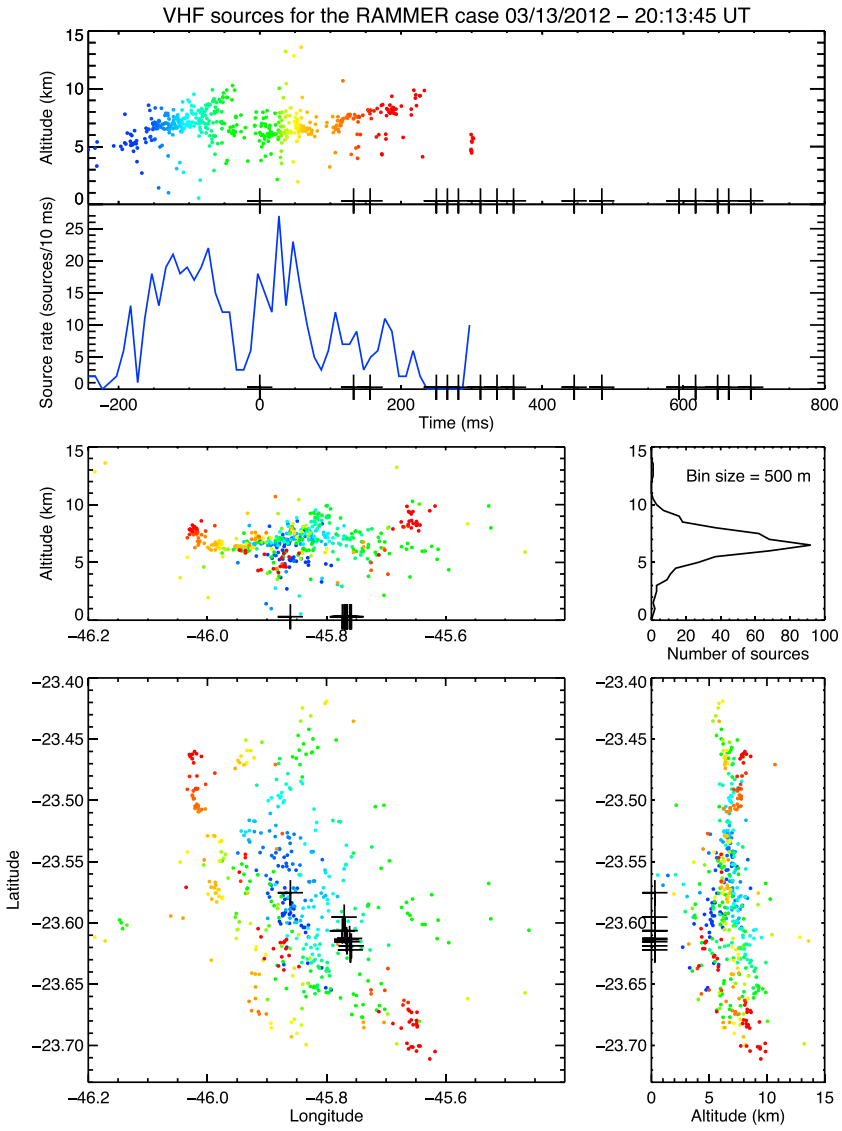

Figure 17. Same as Figure 11 but for the VHF sources detected for Case 2.

4. Discussion

The uniquely visible features (owing mainly to the elevated cloud base in this time frame) of the two bipolar CG flashes analyzed in the present work make it possible to discuss the physical processes responsible for the creation of the subsequent negative strokes. The two cases are distinct in one important aspect: while Case 1 had the negative strokes following the same channel to ground as the initial positive stroke, Case 2 had all the subsequent negative strokes touching ground through a path that was different from the one created by the initial positive stroke. However, the analysis of the high-speed video records shows that in both cases the negative return strokes are initiated by recoil leaders, although in different contexts. Also, the occurrence of these bipolar CG flashes is extremely uncommon, since they can be seen as a subclass of positive CG flashes (already rare), and both events occurred in sequence. The possible explanation for this feature may rely on the thunderstorm itself, which presents evidence of having an inverted polarity structure similar to the trailing stratiform region of squall lines (as discussed by *Williams and Yair* [2006]), such as the following:

1. Evidence of midlevel positive-dominant charge region: VHF data from the SPLMA provided indirect information on the charge distributions within the thunderstorm. Figure 18 shows a map of VHF sources and LLS locations (blue as negative CGs, red as positive CGs, and the bipolar CG flashes in yellow) that were

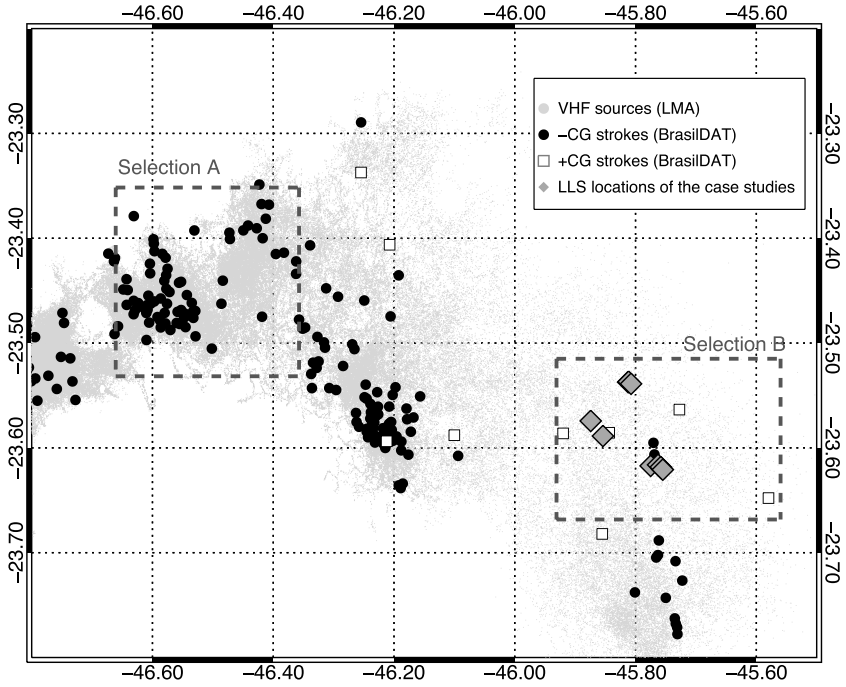

Figure 18. Map of BrasilDAT lightning locations superimposed on LMA VHF sources (gray) detected between 20:10 and 20:40 UT. Black circles are negative strokes, open white squares are positive strokes, and gray diamonds are strokes that belong to the bipolar CG flashes. The dashed squared areas are different data selections for the charge structure analysis.

detected between 20:10 and 20:40 UT. The green selections "A" and "B" drew on the Figure 18 cover the same time period, representing different convective regimes. A is from a regular negative CG-predominant regime, while B is from the positive CG-predominant regime. The graphs of Figure 19 show latitudinally integrated plots of the LMA sources with height for both selections. It is now well established that LMA sources predominate where negative leaders propagate, i.e., in positive-dominant charge regions [*Williams*, 2006]. The differences in the altitude distribution of LMA sources between those plots suggest the presence of a midlevel positive charge region in the case of the predominant positive CG thunderstorm in selection B (where squall line dissipation was noted), in accordance with electric field soundings of Mesoscale Convective System (MCS) stratiform regions presented by *Shepherd et al*. [1996] and *Rust et al*. [2005, Figures 4 and 9].

2. Presence of a low-level negative charge region: The high-speed camera recorded isolated recoil leaders below cloud base on both cases, with predominantly horizontal channels, supportive of stratiform space charges. The corona effect could be responsible for the generation of additional charges on the lower portion of the cloud, analog to the production of the lower screening layer in a regular tripolar structured thunderstorm [*Rakov and Uman*, 2003]. However, in this case, the charges generated by corona are negative due to the main charge region being of positive polarity. On the other hand, *Waldteufel et al*. [1980], during a triggered lightning experiment, reported "air discharges" and suspected that charges drifted to low altitude outside the cloudy or rainy areas were responsible for their observations, also stating that this is not an infrequent feature on thunderclouds.
3. Unusually high rate of positive CG flashes: During the 30 min of observations over selection B area (Figure 18), the cameras recorded four positive and two bipolar CG flashes. The combined information of the LF and VLF networks installed during the CHUVA campaign resulted in eight positive, two negative, and three bipolar flashes, a ratio of 85% of positive and bipolar CG flashes over the total amount of cloud-to-ground lightning. The percentage of positive/bipolar CG flashes produced by that thunderstorm was surprisingly high and does not match the general behavior of a positive/negative CG flash ratio, which is normally around 10% [e.g., *Rakov*, 2003].

With the positive-dominant midlevel charge region, the positive CG flashes are more likely to occur, and, in this case, a probable low-level negative charge region (on the surroundings of cloud base) might have

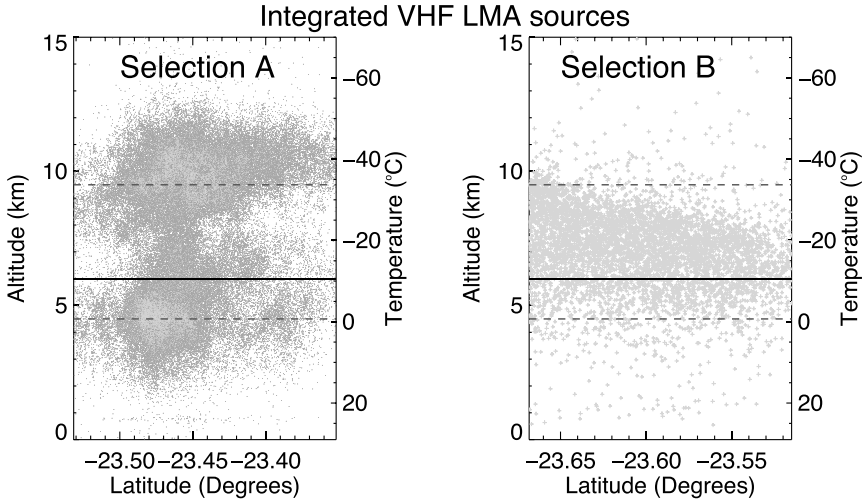

Figure 19. Integrated latitudinal plots of the LMA sources with height for selection A (on the left-hand side) and selection B data (on the right-hand side). In both plots the dashed lines are the mean altitudes of positive-dominant charge regions in a regular tripole configuration. The solid line corresponds to the location of the −10°C isotherm based on a proximity sounding. The exact area and location of each selection (A and B) are shown in Figure 18.

favored the development of low-level recoil leaders, thus enabling the formation of the bipolar CG flashes. A more comprehensive analysis of this thunderstorm will be addressed in detail in a future work.

In Case 1 the recoil leaders retraced a channel branch that was originally ionized by the positive leader that set the stage for the initial positive stroke, as illustrated in Figure 20. All the observed recoil events fit into the phenomenology reported by previous researchers [*Mazur*, 2002; *Williams*, 2006; *Saba et al*., 2008; *Mazur and Ruhnke*, 2011; *Warner*, 2012; *Williams and Heckman*, 2012]; one of them, however, propagates toward ground after it reaches the vertical channel segment, instead of moving upward into the cloud base. This process produces a negative return stroke and is subsequently repeated, generating three additional negative strokes. The genesis of the subsequent negative strokes of Case 1 would have been observed as a regular dart leader that followed a path previously created by a positive stroke if the cloud base were lower. It would be similar to the event analyzed in detail by *Jerauld et al*. [2009], to one of the four events reported by *Fleenor et al*. [2009] or both events described by *Saba et al*. [2012]. The high-speed video data of Case 1 is the first optical evidence that single-channel bipolar CG flashes are produced as consequence of recoil activity. This suggests that the negative strokes in such events are essentially identical to subsequent strokes in negative flashes, as previous VHF observations indicated [e.g., *Shao et al*., 1995; *Rison et al*., 1999].

The large number of recoil leaders that precede the first subsequent stroke (Figure 7) indicates that they have a cumulative effect in reinforcing the heating and ionization of the remnants of the positive leader branch. During the interstroke intervals between the strokes that followed the first negative CG, no recoil activity was observed in those branches, with the exception of the recoil/dart leader sequences that initiated each of those strokes. This suggests that the heating generated through the entire visible channel by the first negative stroke could make it conductive enough for the following recoil/dart leaders to reach ground without the need of previous recoil events to act as their "precursors." The only exception was the fourth (and last) negative stroke. Approximately 25 ms after the third stroke, a recoil leader propagated through the horizontal channel segment, but moving toward the cloud base. The fourth stroke has occurred 15 ms after that, completing the bipolar CG flash after its longest interstroke interval (40 ms).

The analysis of Case 2 suggests that recoil leaders can also be responsible for the creation of a conductive channel for the subsequent negative return strokes that is different from the one followed by the initial positive stroke, possibly after a transition to a stepped propagation mode after leaving the previously ionized channel branches. The high-speed video data show that part of the channel to ground followed by the first subsequent negative stroke was previously illuminated by at least one recoil leader that occurred during

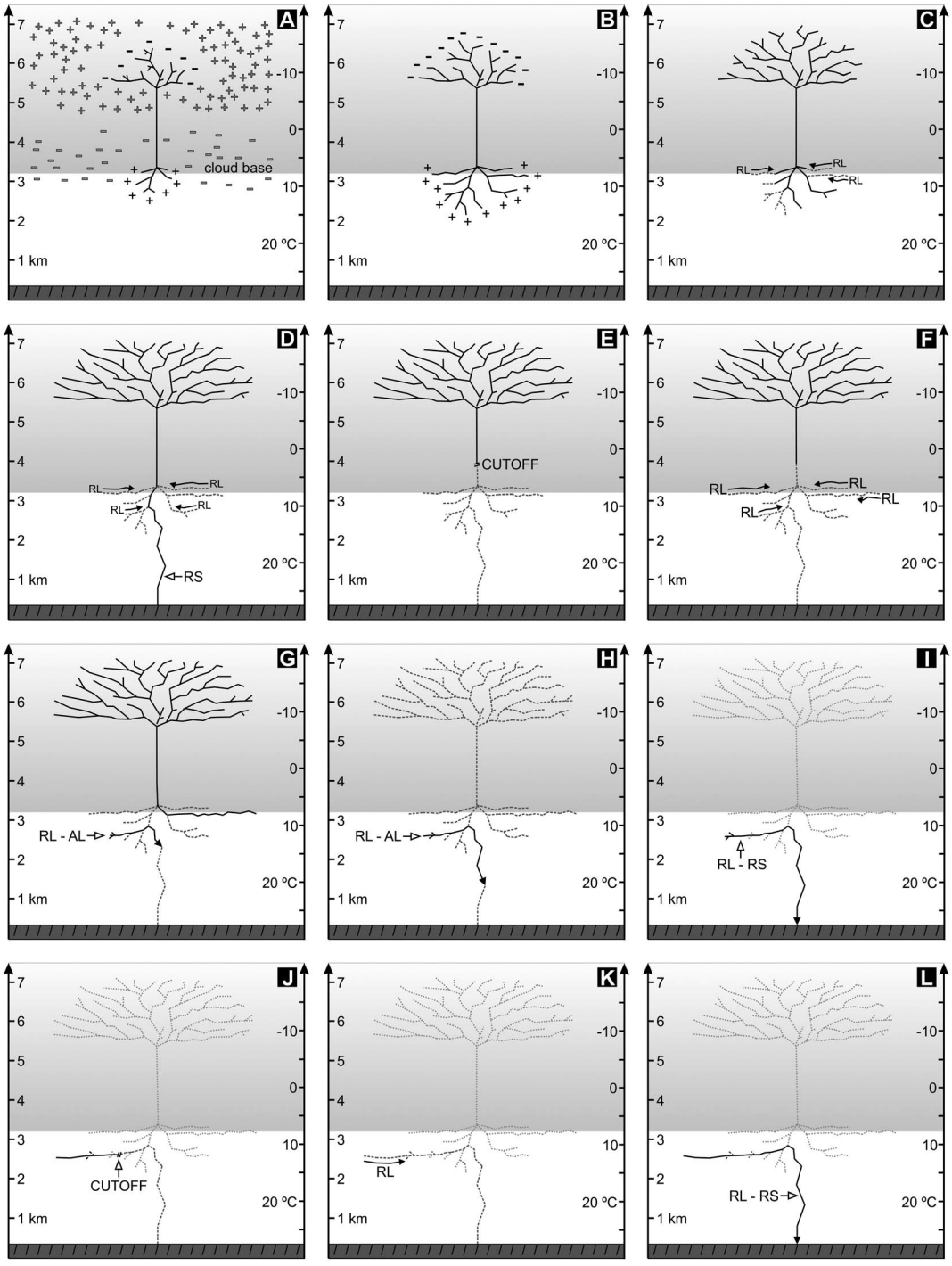

Figure 20. (a–l) Illustration of the mechanism proposed to explain natural bipolar cloud-to-ground flashes. Each panel is discussed in detail in the main text body. The two minus signs represent a single charge region, partially inside the cloud and partially outside the cloud. The elaboration of the figure was based mainly on Case 1 and the main differences found on Case 2 are discussed in section 4 of the paper.

the continuing current period of the initial positive stroke. Instead of reaching the original channel to ground (as observed in Case 1), this recoil/dart leader sequence diverges downward, eventually touching ground on a different contact point and producing a negative return stroke (as shown in Figure 15). If a similar process occurs above cloud base, one would have the situation of three of the four bipolar CG flashes described by *Fleenor et al.* [2009], in which the subsequent negative strokes created new ground contact

points. Unfortunately, there is no available fast electric field data for the leader processes, which would make it possible to see if the recoil/dart leader process propagates in a stepped fashion after it diverges from the previously ionized channel segment. Also, the high-speed camera frame rate was not high enough to provide multiple estimates of propagation speed, which could reveal the presence of a discontinuity in the speed from the early phase (expected to be between 10^6 and 10^7 m s^{-1}, typical of recoil and dart leaders) to the final stages of propagation (during which one would expect stepped leader speeds, typically of the order of 10^5 m s^{-1}) [*Campos et al*., 2014].

Figure 20 illustrates in detail the mechanism proposed to explain both natural bipolar cloud-to-ground flashes described in the present work. Both flashes initiated between 3 and 5 km altitude, where the respective negative- and positive-dominant charge regions were located. The cartoon also indicates the presence of an extended layer of negative space charge below the cloud base, since they are needed to explain the visible horizontal propagation of the leaders/recoil leaders there. It is conceivable that this negative space charge accumulated in the subcloud region from corona discharge from the Earth's surface in the presence of a strong downward directed electric field. Each panel of Figure 20 depicts the following processes:

(a) and (b): The cloud base is located at 3.2 km height, and the flash develops in a bidirectional fashion, with the positive end of the lightning tree propagating toward ground and the negative end developing inside the cloud. The ramifications in the positive end are usually fainter than in the negative end and are barely visible with the camera.

(c): The recoil leaders seem to take place when the faintest branches are about to stop their development for any reason, for example, when a current cutoff happened at some point. The recoils act like a current surge on the branch, extending it a little further, and then, the branch can propagate for itself again. Such bidirectional nature of the recoil leaders has been previously documented in detail by *Warner et al*. [2012] and *Mazur et al*. [2013]. This process can occur on several branches and can repeat on the same one multiple times.

(d): The lower end of the bidirectional leader continues to propagate until it touches ground, producing the initial positive return stroke. It is followed by a period of continuing current, which takes place simultaneously with recoil leader activity on positive leader branches that have been cutoff once the return stroke occurred.

(e): Once the continuing current is finished, the lower section of the double-ended tree is presumed to be cut off from the in-cloud negative end. The positive charge transfer to ground stops, but the negative end of the in-cloud lightning tree continues to develop independently.

(f): A large number of recoil leaders (indicated as RL) occur in channel branches visible below cloud base that were previously ionized by the positive leader. Some can reconnect with the active in-cloud negative leader, forming an intracloud discharge, and others are not able to do so.

(g) and (h): Some of the recoil leaders, in particular, develop toward the vertical section of the channel to ground followed by the positive stroke, behaving as attempted leaders (indicated as RL-AL). Eventually, the in-cloud negative leader propagation is interrupted, as indicated by the VHF sources detected by the SPLMA (Figure 11).

(i): One of the recoil leaders (that occurred in the region considered for the graph of Figure 7) was capable of following the same path to ground as the initial positive stroke. It behaved as a regular dart leader and produced the first subsequent negative return stroke (indicated as RL-RS). It is important to notice that, from this point on, the horizontal end of the channel carries positive charges, and the descending channel carries negative charges to ground.

(j): Negative charge transfer to ground is finished after the channel cutoff. The positive horizontal end, however, continues to propagate with a luminous emission below the camera sensitivity. As shown previously, the main evidence of this continuous development between strokes is the approximately uniform channel extension documented in Figure 10 (and Figure 16 for Case 2).

(k): At some point the positive leader propagation is terminated due to current cutoff. This allows the initiation of another recoil leader, which propagates bidirectionally toward ground (similarly to the initial positive and the first negative subsequent strokes) at the same time as it develops further the horizontal positive end of the channel.

(l): The negative end of the recoil leader reaches ground and produces the second negative stroke, behaving as a regular dart leader. After the first negative return stroke, no intense recoil activity was presented on that branch, and each new recoil leader was responsible for another negative return stroke. The new channel

behaves like a regular negative flash, but at a smaller scale. Recoil leaders will continue to produce additional negative strokes as long as charges are still available around the positive leader and while the channel length remains stable.

The conditions for the production of new negative strokes are supported by the charge transfers measured by *Waldteufel et al*. [1980] through field-mill records and by the channel stability model introduced by *Heckman* [1992] and further developed by *Williams and Heckman* [2012]. *Waldteufel et al*. [1980] reported a triggered lightning event in which 10 return strokes were initiated in a region of clear air, below cloud base. Also, from stroke to stroke, the illuminated channel branches developed spatially, reaching up progressively into the charge region with an estimated speed of 3×10^4 m s^{-1}. They interpreted the observations as a positive leader constantly propagating upward, neutralizing the negative charge distribution located below cloud base by means of both leader development and return stroke occurrence. It is reasonable to assume that a similar phenomenon occurred in the events described here, with the horizontal positive leader developing for as long as there was a negative charge distribution below cloud base not only to feed the propagation but also to produce an adequate electric field and to be transferred to ground by each subsequent negative stroke. Also, the channel stability models by *Heckman* [1992] and *Williams and Heckman* [2012] suggest that the relationship between the total channel length and its current also plays an important role on whether or not additional strokes may occur and/or they might develop continuing currents. It is reasonable to assume that the combination of the tendency toward the less stable regime of the current versus length diagram of *Heckman* [1992] with the decrease of negative charge availability (similarly to what was observed by *Waldteufel et al*. [1980]) eventually limited the number of subsequent negative strokes. The model predictions were obtained by assuming that a lightning channel possesses the negative differential resistance observed in laboratory arcs produced in the air, i.e., at low currents (generally below 100 A) the voltage drop across the channel increases as current decreases [*King*, 1961]. At the moment, however, there are no measured parameters to test these ideas quantitatively.

Figures 20h to 20l show the scenario of Case 1, which is valid for bipolar CG flashes where strokes of both polarities follow the same channel to ground. Case 2 presented a very similar development as Case 1, the only difference being the fact that the strike points of the subsequent negative strokes followed a different path to ground. The behavior presented in Figures 20a through 20f is exactly the same, but the processes illustrated from Figure 20g onward have some crucial differences. In Case 2, a very large branch presented recoil activity far from the main channel. When the recoil traced back the branch, it diverged to ground in the form of a stepped leader, instead of remaining on the main channel. That created the first negative stroke (equivalent to Figures 20 through 20i). All 14 subsequent strokes followed the same path to ground from that point on, cycling through the processes of Figures 20j to 20l following the new ground termination created by the recoil/dart-stepped leader sequence of the first subsequent negative stroke.

Given the recent high-speed video records with evidence that recoil leaders propagate in a bidirectional fashion [*Warner et al*., 2012; *Mazur et al*., 2013], the authors suggest that the recoil/dart leader sequence that produces each negative stroke further extends the horizontal channel segment from where it originates. Eventually, current cutoff occurs, interrupting charge transfer to ground after the negative stroke. However, it seems that the positive leader at the upper end of the channel continues to propagate horizontally, and this action may serve to restress the cutoff segment to new breakdown. This is suggested by the temporal evolution of the visible channel length, which occurs repeatedly at a rate of 10^4 m s^{-1} between subsequent strokes (Figures 10, 16, and 20j). Additionally, *Waldteufel et al*. [1980] observed a remarkably similar behavior (as commented earlier in this section) and *Mazur* [2002, section 2.2 and Figure 5] describes the same behavior for the "development of the unidirectional positive leader, which continues even after current cutoff" right after a return stroke in a regular negative cloud-to-ground flash. Eventually, the positive leader development is interrupted by cutoff, giving rise to the inception of other recoil leaders (Figure 20k). These recoil leaders, as both case studies have shown, retrace the whole channel to ground and set the stage for the subsequent negative strokes (Figure 20l).

5. Concluding Remarks

This work analyzes two temporally close bipolar cloud-to-ground flashes observed in São José dos Campos, southeastern Brazil, during the summer of 2012. One high-speed camera of the RAMMER network and several

other instruments installed during that summer, as part of the CHUVA campaign, observed these events. Due to the elevated cloud base height, the cameras were able to record the entire development of the subsequent negative strokes below cloud base in both cases. Also, each case presented different behaviors: while in Case 1 all subsequent strokes shared the same final channel section to ground, Case 2 had different ground contact points for the main positive CG stroke and the subsequent negative CG strokes. The joint analysis of the high-speed camera, LMA, and LLS data allowed the elaboration of a conceptual empirical inception mechanism of subsequent negative strokes in natural downward bipolar flashes (Figure 20). The main results were as follows:

1. The first optical evidence that both single- and multiple-channel bipolar flashes occur as a consequence of recoil leader activity in the branches of the initial positive return stroke.
2. The total channel length of the negative strokes increased progressively with time. The channel growth rate was equivalent to a propagation speed of the order of 10^4 m s^{-1}. Such speed corresponds to positive leaders observed under many different circumstances. The most probable mechanism is that the positive end of the leader continuously propagates until the point where it becomes faint and eventually stops, possibly due to current cutoff.
3. At the verge of a channel current cutoff or after the cutoff has taken place, recoil leaders might act on the channels like current surges, feeding the channel and also extending it a little further. From that point on, the channel can continue the self-propagation, produce more recoil leaders, or completely fade away and stop its extension.
4. By analyzing the LMA data it was possible to show that all the subsequent strokes had no connection with the upper in-cloud negative leader created during the bidirectional development of the initial return stroke.

Cases 1 and 2 also presented a few different features, such as the following:

1. Case 1: A large number of recoil leaders (close to twenty) occurred after the initial positive stroke until one of them could strike ground. This indicates that the cumulative effect of ionization and heating by the developing recoil leaders was important in creating the adequate conditions for one of them to produce finally a negative stroke.
2. Case 2: In this case, however, the recoil/dart leader in development leaves the original path, creating a new branch and eventually contacting ground.

Even though this mechanism was proposed based on two events whose negative strokes had their preparatory process observed by a high-speed camera below cloud base, it can also be extended to the more general case of bipolar CG flashes. All the natural cloud-to-ground events that have been reported previously [*Fleenor et al*., 2009; *Jerauld et al*., 2009; *Saba et al*., 2012] can be described by this mechanism if one considers that the recoil leaders responsible for the subsequent negative strokes also occur above cloud base. Additionally, considering the current knowledge of the bidirectional leader model and how it explains the formation of subsequent strokes in ordinary negative cloud-to-ground flashes [e.g., *Mazur*, 2002; *Williams and Heckman*, 2012], the case studies of the present work also support the suggested mechanism for that type of event. In this case, the recoil leader occurs in a cutoff segment of the in-cloud positive end of the bidirectional leader, eventually propagating all the way to ground and producing a subsequent negative stroke.

The SPLMA data were also vital in obtaining evidence for a dipole structure in the storm producing the two bipolar CG flashes, similar to the inverted polarity thunderstorms reported in the literature. The majority of VHF sources in that cell were located between 5 and 10 km of altitude for 30 min, indicating that there was a predominance of positive charges within that range. The differences between these two profiles suggest that the bipolar CG flashes occurred in an inverted dipole situation. This uncommon structure could have favored not only the occurrence of bipolar cloud-to-ground discharges but also positive flashes, as recorded by the same high-speed camera and the LLS afterward, over a period of roughly 18 min.

Acknowledgments

The authors would like to thank FAPESP for their financial support under the projects 08/56711-4 and 2010/01742-2. This work was also partially supported by the CHUVA project (project FAPESP 2009/15235-8). We specially thank UNIVAP (Universidade do Vale do Paraíba) and Rede Vanguarda de Televisão for their support in hosting the sensors during the observations and helping with maintenance. The authors are also grateful to all CHUVA participants responsible for the installation and maintenance of the several sensors present at the 2012 campaign and whose data were vital to the development of this work.

References

Bailey, J. C., L. D. Carey, R. J. Blakeslee, S. J. Goodman, R. Albrecht, C. A. Morales, and O. Pinto Jr. (2011), São Paulo Lightning Mapping Array (SP-LMA): Deployment and plans, paper presented at the XIV International Conference on Atmospheric Electricity, Rio de Janeiro, Brazil.

Berger, K., and E. Vogelsanger (1965), Messungen und Resultate der Blitzforschung der Jahre 1955–1963 auf dem Monte San Salvatore, *Bull. Schweiz. Eletrotech. Ver.*, *56*, 2–22.

Berger, K., and E. Vogelsanger (1966), Photographische Blitzuntersuchungen der Jahre 1955–1963 auf dem Monte San Salvatore, *Bull. Schweiz. Elektrotech. Ver.*, *57*, 599–620.
Betz, H.-D., K. Schmidt, W. P. Oettinger, and M. Wirz (2004), Total VLF/LF-lightning and pseudo 3D-discrimination of intra-cloud and cloud-to-ground discharges, paper presented at 18th International Lightning Detection Conference, Vaisala, Helsinki, Finland.
Campos, L. Z. S., M. M. F. Saba, O. Pinto Jr., and M. G. Ballarotti (2009), Waveshapes of continuing currents and properties of M-components in natural positive cloud-to-ground lightning, *Atmos. Res.*, *91*, 416–424, doi:10.1016/j.atmosres.2008.02.020.
Campos, L. Z. S., J. Alves, A. C. V. Saraiva, E. R. Williams, and O. Pinto Jr. (2013), On the relation between return stroke peak current provided by lightning location systems and its peak luminosity obtained from high-speed video cameras: Preliminary results, paper presented at CHUVA International Workshop, Nat. Inst. Space Res., São Paulo, Brazil.
Campos, L. Z. S., M. M. F. Saba, T. A. Warner, O. Pinto Jr., E. P. Krider, and R. E. Orville (2014), High-speed video observations of natural cloud-to-ground lightning leaders—A statistical analysis, *Atmos. Res.*, *135–136*, 285–305, doi:10.1016/j.atmosres.2012.12.011.
Cummins, K. L., M. J. Murphy, E. A. Bardo, W. L. Hiscox, R. B. Pyle, and A. E. Pifer (1998), A combined TOA/MDF technology upgrade of the U.S. National Lightning Detection Network, *J. Geophys. Res.*, *103*, 9053–9044.
Demetriades, N. W. S., M. J. Murphy, and J. A. Cramer (2010), Validation of Vaisala's Global Lightning Dataset (GLD360) over the continental United States, paper presented at 21st International Lightning Detection Conference, Vaisala, Orlando, Fla.
Fleenor, S. A., C. J. Biagi, K. L. Cummins, E. P. Krider, and X. M. Shao (2009), Characteristics of cloud-to-ground lightning in warm-season thunderstorms in the Central Great Plains, *Atmos. Res.*, *91*, 333–352, doi:10.1016/j.atmosres.2008.08.011.
Heckman, S. (1992), Why does a lightning flash have multiple strokes?, PhD thesis, Massachusetts Inst. of Technol., Cambridge.
Hubert, P., A. Eybert-Berard, and L. Barret (1984), Triggered lightning in New Mexico, *J. Geophys. Res.*, *89*, 2511–2521, doi:10.1029/JD089iD02p02511.
Idone, V. P., R. E. Orville, D. M. Mach, and W. D. Rust (1987), The propagation speed of a positive lightning return stroke, *Geophys. Res. Lett.*, *14*, 1150–1153, doi:10.1029/GL014i011p01150.
Jerauld, J. E., M. A. Uman, V. A. Rakov, K. J. Rambo, D. M. Jordan, and G. H. Schnetzer (2009), Measured electric and magnetic fields from an unusual cloud-to-ground lightning flash containing two positive strokes followed by four negative strokes, *J. Geophys. Res.*, *114*, D19115, doi:10.1029/2008JD011660.
Jordan, D. M., V. P. Idone, V. A. Rakov, M. A. Uman, W. H. Beasley, and H. Jurenka (1992), Observed dart leader speed in natural and triggered lightning, *J. Geophys. Res.*, *97*, 9951–9957, doi:10.1029/92JD00566.
Kasemir, H. W. (1950), Qualitative Ubersicht uber Potential-, Feld- und Ladungsverhaltnisse bei einer Blitzentladung in der Gewitterwolke, in *Das Gewitter*, edited by H. Israel, pp. 112–126, Akad. Verlagsges, Leipzig, Germany.
Kasemir, H. W. (1960), A contribution to the electrostatic theory of a lightning discharge, *J. Geophys. Res.*, *65*, 1873–1878, doi:10.1029/JZ065i007p01873.
King, L. A. (1961), The voltage gradient of the free burning arc in air or nitrogen, paper presented at 5th International Conference on Ionization Phenomena in Gases, Munich, Germany.
Kitagawa, N., and K. Michimoto (1994), Meteorological and electrical aspects of winter thunderclouds, *J. Geophys. Res.*, *99*, 10,713–10,721, doi:10.1029/94JD00288.
Kito, Y., K. Horii, Y. Higashiyama, and K. Nakamura (1985), Optical aspects of winter lightning discharges triggered by the rocket-wire technique in Hokuriku district of Japan, *J. Geophys. Res.*, *90*, 6147–6157, doi:10.1029/JD090iD04p06147.
Kong, X., X. Qie, and Y. Zhao (2008), Characteristics of downward leader in a positive cloud-to-ground flash observed by high-speed video camera and electric field changes, *Geophys. Res. Lett.*, *35*, L05816, doi:10.1029/2007GL032764.
Krehbiel, P. R. (1981), An analysis of the electric field change produced by lightning, PhD thesis, Dep. of Pure and Appl. Phys., Univ. Manchester, Manchester, England.
Krehbiel, P. R., M. Brook, and R. A. McCrory (1979), An analysis of the charge structure of lightning discharges to ground, *J. Geophys. Res.*, *84*, 2432–2456, doi:10.1029/JC084iC05p02432.
Krider, E. P. (1974), An unusual photograph of an air lightning discharge, *Weather*, *29*, 24–27.
Les Renardières Group (1977), Positive discharges in long air gaps at Les Renardières, 1975 results and conclusions, *Electra*, *53*, 31–153.
Machado, L. A. T., A. Calheiros, E. Mattos, I. Costa, D. Vila, R. Albrecht, C. Morales, C. Angelis, M. Silva Dias and G. Fisch (2012), Tropical cloud processes: First results from CHUVA Project, paper presented at 16th International Conference on Clouds and Precipitation (ICCP2012), Leipzing, Germany.
Mazur, V. (2002), Physical processes during the development of lightning flashes, *C. R. Phys.*, *3*, 1393–1409.
Mazur, V., and L. H. Ruhnke (2011), Physical processes during development of upward leaders from tall structures, *J. Electrostat.*, *69*, 97–110, doi:10.1016/j.elstat.2011.01.003.
Mazur, V., L. H. Ruhnke, T. A. Warner, and R. E. Orville (2013), Recoil leader formation and development, *J. Electrostat.*, doi:10.1016/j.elstat.2013.05.001, in press.
McEachron, K. B. (1939), Lightning to the Empire State Building, *J. Franklin Inst.*, *227*, 149–217.
Naccarato, K. P.; A. C. V. Saraiva, M. M. F. Saba, C. Schumann and O. Pinto Jr. (2012), First performance analysis of BrasilDAT total lightning network in southeastern Brazil, paper presented at International Conference On Grounding and Earthing (GROUND'2012), Bonito, Brazil.
Nag, A., and V. A. Rakov (2012), Positive lightning: An overview, new observations, and inferences, *J. Geophys. Res.*, *117*, D08109, doi:10.1029/2012JD017545.
Nakahori, K., T. Egawa, and H. Mitani (1982), Characteristics of winter lightning currents in Hokuriku district, *IEEE Trans. Power Appar. Syst.*, *101*, 4407–4412.
Orville, R. E., and V. P. Idone (1982), Lightning leader characteristics in the Thunderstorm Research International Program (TRIP), *J. Geophys. Res.*, *87*, 11,177–11,192, doi:10.1029/JC087iC13p11177.
Rakov, V. A. (2003), A review of positive and bipolar lightning discharges, *Bull. Am. Meteorol. Soc.*, *84*, 767–776, doi:10.1175/BAMS-84-6-767.
Rakov, V. A., and M. A. Uman (2003), *Lightning: Physics and Effects*, Cambridge Univ. Press, New York.
Rison, W., R. J. Thomas, P. R. Krehbiel, T. Hamlin, and J. Harlin (1999), A GPS-based three-dimensional lightning mapping system: Initial observations in central New Mexico, *Geophys. Res. Lett.*, *26*, 3573–3576, doi:10.1029/1999GL010856.
Rust, W. D., D. R. MacGorman, E. C. Bruning, S. A. Weiss, P. R. Krehbiel, R. J. Thomas, W. Rison, T. Hamlin, and J. Harlin (2005), Inverted-polarity electrical structures in thunderstorms in the Severe Thunderstorm Electrification and Precipitation Study (STEPS), *Atmos. Res.*, *76*, 247–271, doi:10.1016/j.atmosres.2004.11.029.
Saba, M. M. F., K. L. Cummins, T. A. Warner, E. P. Krider, L. Z. S. Campos, M. G. Ballarotti, O. Pinto Jr., and S. A. Fleenor (2008), Positive leader characteristics from high-speed video observations, *Geophys. Res. Lett.*, *35*, L07802, doi:10.1029/2007GL033000.
Saba, M. M. F., W. Schulz, T. A. Warner, L. Z. S. Campos, C. Schumann, E. P. Krider, K. L. Cummins, and R. E. Orville (2010), High-speed video observations of positive lightning flashes to ground, *J. Geophys. Res.*, *115*, D24201, doi:10.1029/2010JD014330.

Saba, M. M. F., C. Schumann, T. A. Warner, W. Schulz, and R. E. Orville (2012), Bipolar cloud-to-ground flashes observations, paper presented at 31st International Conference on Lightning Protection, Austrian Electrotech. Assoc., Vienna, Austria.

Saraiva, A. C. V., O. Pinto Jr, M. Ferreira, G. S. Zepka, and M. M. F. Saba (2011), RAMMER Project: First observations of the high speed camera network to monitor and study lightning, paper presented at the XIV International Conference on Atmospheric Electricity, Rio de Janeiro, Brazil.

Schonland, B. F. J., D. J. Malan, and H. Collens (1935), Progressive lightning, 2, *Proc. R. Soc. London*, *A152*, 595–625.

Schulz, W., and G. Diendorfer (2003), Bipolar flashes detected with lightning location systems and measured on an intrumented tower, paper presented at the VII International Symposium on Lightning Protection, Curitiba, Brazil.

Shao, X. M., P. R. Krehbiel, R. J. Thomas, and W. Rison (1995), Radio interferometric observations of cloud-to-ground lightning phenomena in Florida, *J. Geophys. Res.*, *100*, 2749–2783, doi:10.1029/94JD01943.

Shepherd, T. R., W. D. Rust, and T. C. Marshall (1996), Electric fields and charges near 0°C in stratiform clouds, *Mon. Weather Rev.*, *124*, 920.

Vonnegut, B., and C. B. Moore (1958), Giant electrical storms, in *Recent Advances in Atmospheric Electricity*, edited by L. G. Smith, pp. 399–411, Pergamon Press, New York.

Waldteufel, P., P. Metzger, J.-L. Boulay, P. Laroche, and P. Hubert (1980), Triggered lightning strokes originating in clear air, *J. Geophys. Res.*, *83*, 2861–2868, doi:10.1029/JC085iC05p02861.

Warner, T. A. (2012), Observations of simultaneous upward lightning leaders from multiple tall structures, *Atmos. Res.*, *117*, 45–54, doi:10.1016/j.atmosres.2011.07.004.

Warner, T. A., M. M. F. Saba, and R. E. Orville (2012), Characteristics of upward leaders from tall towers, paper presented at 22nd International Lightning Detection Conference, Vaisala, Broomfield, Colo.

Williams, E., and S. Heckman (2012), Polarity asymmetry in lightning leaders: The evolution of ideas on lightning behavior from strikes to aircraft, *AerospaceLab J.*, *5*, AL05–04.

Williams, E., and Y. Yair (2006), The microphysical and electrical properties of sprite-producing thunderstorms, in *Sprites, Elves and Intense Lightning Discharges*, edited by M. Füllekrug et al., pp. 57–83, Springer, Dordrecht, Netherlands, doi:10.1007/1-4020-4629-4_3.

Williams, E. R. (2006), Problems in lightning physics—The role of polarity asymmetry, *Plasma Sources Sci. Technol.*, *15*, S91–S108, doi:10.1088/0963-0252/15/2/S12.

Williams, E. R., and D. J. Boccippio (1993), Dependence of cloud microphysics and electrification on mesoscale vertical air motion in stratiform precipitation, paper presented at the Conference on Atmospheric Electricity, pp. 825–831, Am. Meteorol. Soc., St. Louis, Mo.

Zipser, E. J. (1977), Mesoscale and convective-scale downdrafts as distinct components of squall-line structure, *Mon. Weather Rev.*, *105*, 1568–1589, doi:10.1175/1520-0493(1977)105<1568:MACDAD>2.0.CO;2.